ISSN 1027-5495. Functional Materials, 30, No.2 (2023), p. 178-186.
doi:https://doi.org/10.15407/fm30.02.178

Investigation of the effect of processing parameters on the spectroscopic properties of ZnSe NCs for hot-pressed ceramics of the Cleartran and Multispectral classes

***Ye.G.Plakhtii*[1], *D.B.Hlushkova*[2], *V.M.Volchuk*[1], *V.V.Slavnyi*[3], *S.V.Demchenko*[2], *V.A.Saenko*[2]**

[1]Prydniprovska State Academy of Civil Engineering and Architecture, 24a Chernyshevsky Str., 49000 Dnipro, Ukraine
[2]Kharkiv National Automobile and Highway University, 25 Yaroslava Mudrogo Str., 61002 Kharkiv, Ukraine
[3]Oles Honchar Dnipro National University, 72 Gagarin Ave., 49010 Dnipro, Ukraine

Received February 20, 2023

ZnSe nanocrystals were synthesized by the combustion synthesis method (self-propagating high temperature synthesis) with different initial current pulses. Annealing was carried out in the temperature range T = 200÷800°C with a step of T = 100°C at atmospheric pressure, in air or in nitrogen. The results of electron micrographs, EPR, XRD analysis and photoluminescence depending on the annealing temperature in air or nitrogen are presented. The dependences of the resonance value of the EPR magnetic field of Mn^{2+} ions, the hyperfine structure constant A of the EPR spectrum of Mn^{2+} ions, the location of the maximum and the half-width of the integral photoluminescence spectrum on the annealing temperature in air or in nitrogen were obtained. After annealing the nanocrystal size increases by ~ 20 %, the fraction of the cubic phase and the lattice parameter of nanocrystals increase, and both the number of dislocations and microstresses decrease compared to the initial charge. For the synthesis of ZnSe nanocrystals with a more perfect structure, it is recommended to use a current pulse of ~ 40 A followed by annealing at T = 800°C in nitrogen. The obtained results make it possible to use the ZnSe nanocrystals synthesized by the combustion method for various optoelectronic devices or for producing hot-pressed ceramics of the Cleartran or Multispectral classes.

Keywords: ZnSe nanocrystals, combustion synthesis method, annealing, EPR, Multispectral classes.

Дослідження впливу параметрів обробки на спектроскопічні властивості НК ZnSe для гарячепресованої кераміки класів Cleartran та Multispectral. *Є.Г.Плахтій, Д.В.Глушкова, В.М.Волчук, В.В.Славний, С.В.Демченко, В.А.Саєнко*

Нанокристали ZnSe синтезовано методом горіння з різними початковими струмовими імпульсами. Відпали проводили в інтервалі температур T = 200÷800°C з кроком T = 100°C при атмосферному тиску, в середовищі повітря або азоту. Наведено результати електронних мікрофотографій, ЕПР, рентгенодифракційного аналізу, фотолюмінесценції залежно від температури відпалу в середовищі повітря або азоту. Отримано залежність резонансного значення магнітного поля ЕПР іонів Mn^{2+}, константи A надтонкої структури спектру ЕПР іонів Mn^{2+}, розташування максимуму та напівширини інтегрального спектру фотолюмінесценції від температури відпалу в середовищі повітря або азоту. При відпалі зростає розмір нанокристалів ~ 20 %, збільшується частка

кубічної фази, збільшується параметр решітки НК, зменшується кількість дислокацій та мікронапруження порівняно з вихідною шихтою. Для синтезу нанокристалів ZnSe з досконалішою структурою рекомендовано використовувати струмовий імпульс ~ 40 А, а далі проводити відпал при температурі T = 800°С в середовищі азоту. Отримані результати дозволяють використовувати нанокристали ZnSe синтезовані методом горіння для різних пристроїв оптоелектроніки або отримання гарячепресованої кераміки класів Cleartran або Multispectral.

1. Introduction

The development of new materials, their processing modes and operating conditions are due to modern requirements of scientific and technological progress [1]. One of the most promising materials with a wide range of applications is zinc selenide. Nanostructures based on ZnSe have found the widest application in LEDs [2, 3], photodetectors, and alpha, gamma, and X-ray detectors [4, 5], field emitters [6, 7], sensors [8, 9], lasers [10, 11], photocatalysis [12, 13], solar cells [14, 15], infrared windows [16, 17], biomedical application[18, 19] etc.

Currently, one of the main tasks of materials science is to obtain nanosized materials with desired properties. There are a large number of methods for the synthesis of nanocrystals (NC): MBE, ALE, MOCVD, VPE, CVD, solution-based techniques, reduction, thermal decomposition, hydrothermal process, printing, hydrolysis, alcoholysis, etc. [2, 20–27]. These methods are of great research interest due to their efficiency in the synthesis of NCs with good size control; many of them have the advantage of low synthesis temperature or technological flexibility. However, the production of NCs by all of the above methods has some disadvantages, such as high cost and rather high complexity of synthesis.

The simplification of the synthesis of nanostructures, the reduction in the cost of synthesis processes, low energy consumption per unit of production, simplicity of the used equipment, its environmental safety, the possibility of creating flexible technologies that easily switch from obtaining some materials to obtaining others on the same equipment are important tasks of materials science [28, 29]. All these tasks and even more are solved by the combustion synthesis method. The main disadvantages of this method are the practical impossibility of obtaining crystals smaller than 50–100 nm, the need for strict control over the reaction, and the possible compaction of samples [28, 29]. However, recent works have shown how easy it is to obtain nanocrystals up to 4 nm in size from nanocrystals obtained by combustion synthesis [30]; this further increases the expediency of obtaining ZnSe NCs by the combustion synthesis method and studying the features inherent in this method. Some foreign researchers and we have already presented the synthesis of ZnSe nanocrystals by the combustion synthesis method earlier [31–34], however, many important issues regarding the structure, EPR spectra, annealing behavior and application of ZnSe NCs have not been previously considered.

2. Experimental

Synthesis of NC ZnSe was carried out according to the method described in [33]. ZnSe and ZnSe:Mn NCs were synthesized in a quartz ampoule placed in a steel reactor with a tight seal. High-purity powders of Zn and Se were taken with a 5 % excess of Se over the stoichiometric composition due to high volatility of selenium during synthesis. In the initial powders, the average particle size ranged from 1 to 5 microns. To optimize the mixing process and average the particle size, the charge was first mixed with ethyl alcohol for one hour. The mixture was then dried for 30 minutes at T ~ 350 K. We would like to clarify that the synthesis reaction was initiated by a current pulse with an amplitude of ~ 35 A or ~ 40 A. The synthesis was carried out at atmospheric pressure in air. Annealing was carried out in the temperature range T = 200–800°C with a step T = 100°C at atmospheric pressure in air or nitrogen.

After obtaining, the powder was sifted through a fine-mesh sieve with a mesh size of 0.5 mm to remove large fractions. For X-ray diffraction analysis (XRD) analysis, the powder was additionally sifted through a fine mesh sieve with a mesh size of 0.15 mm and placed into a special cuvette. XRD of the obtained powder was performed on a DRON-2 diffractometer using Co K_α radiation. For EPR analysis, the powder was placed in a quartz ampoule. The EPR spectrum was studied using a Radiopan SE/X-2543 radiospectrometer. For an electron microscope, a pre-ground sample was applied to a quartz substrate coated with silver to eliminate charging effects. The im-

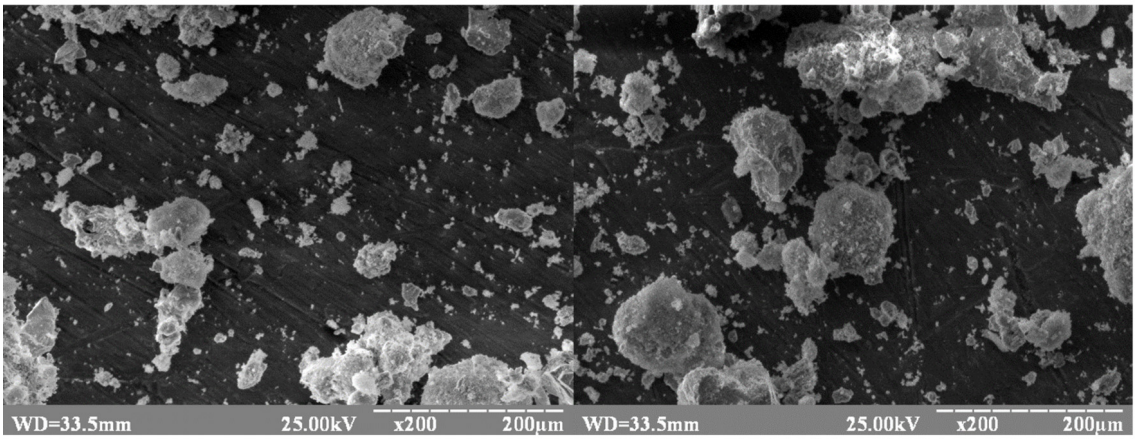

Fig. 1. Electron micrographs of ZnSe NC synthesized at a current of ~ 35 A; before annealing (a) and after annealing (b).

ages of nanoparticles were obtained using a scanning electron microscope REMMA-102-02. Photoluminescence (PL) of NC was excited by emission of a semiconductor laser (λ_{ex} = 3.04 eV). The PL spectra were recorded according to the standard procedure at room temperature; a photomultiplier-136 was used as a radiation detector.

3. Results and discussion

The ZnSe NCs synthesized as a result of combustion synthesis (CS) were a powder, which appearance is shown in Fig. 1. The XRD data show that this powder consisted of polycrystals with mixed crystalline structure and average particle sizes ~ 1–5 μm, which, in their turn, consisted of NCs. The XRD data [33] show that this powder consisted of NCs with mixed crystalline structure. The size of obtained polycrystals correlates with the sizes of particles put in the initial charge. Rapid cooling of the obtained final product can be used to reduce these sizes. It will weaken the process of NC splicing. Also, etching of the final product in 1 % aqueous solution of HNO_3 and H_2O_2 mixture during 20 min may be used to decrease the NC size which was suggested in [30].

To improve the structure and photoluminescence properties of ZnSe NCs, a series of annealings in air and nitrogen vapors was carried out. The duration of each annealing was 30 minutes, the cooling of the samples occurred naturally in the annealing medium.

Figure 2 shows the EPR spectra of ZnSe NCs synthesized at a current strength of ~ 35 A. When these ZnSe NCs are annealed in air, the presence of one hyperfine structure is observed over the entire temperature range studied. It consists of six equidistant lines (1) characteristic of paramagnetic Mn^{2+} centers and a wide EPR spectrum (2) (hereinafter, spectrum types (1) and (2)). The (1) type signal is associated mainly with Mn^{2+} ions built into the cubic lattice, while the (2) type signal (~ 470 G wide) is usually associated with a strong dipole-dipole interaction between neighboring manganese ions. This signal may originate from a Mn pair or a cluster [36].

A decrease in the intensity of the (1) type spectrum and an increase in the intensity of the (2) type spectrum occur unevenly. The intensity of the (1) type EPR spectrum during annealing at T = 200 and 300° changes insignificantly compared to the initial spectrum. This indicates that the structure of the ZnSe nanocrystals, and in particular, the number of dislocations, does not change during annealing at these temperatures. On passing from T = 300°C to T = 400°C, the intensity of the EPR spectrum of Mn^{2+} ions of type (1) decreases by almost one and a half times and a signal of the (2) type appears; this fact may indicate the beginning of the movement of dislocations and the formation of more energetically beneficial structures. The intensity of spectra of both (1) and (2) types changes insignificantly in the range T = 400*div*600°C. In the temperature range T = 400÷600°C, to the left of the six lines of the hyperfine structure of Mn^{2+} ions, additional lines appear, which are characteristic of bulk ZnSe crystals. This indicates, most likely, a sharp growth and association of crystallites, accompanied by a change in the structure of the samples in this temperature range.

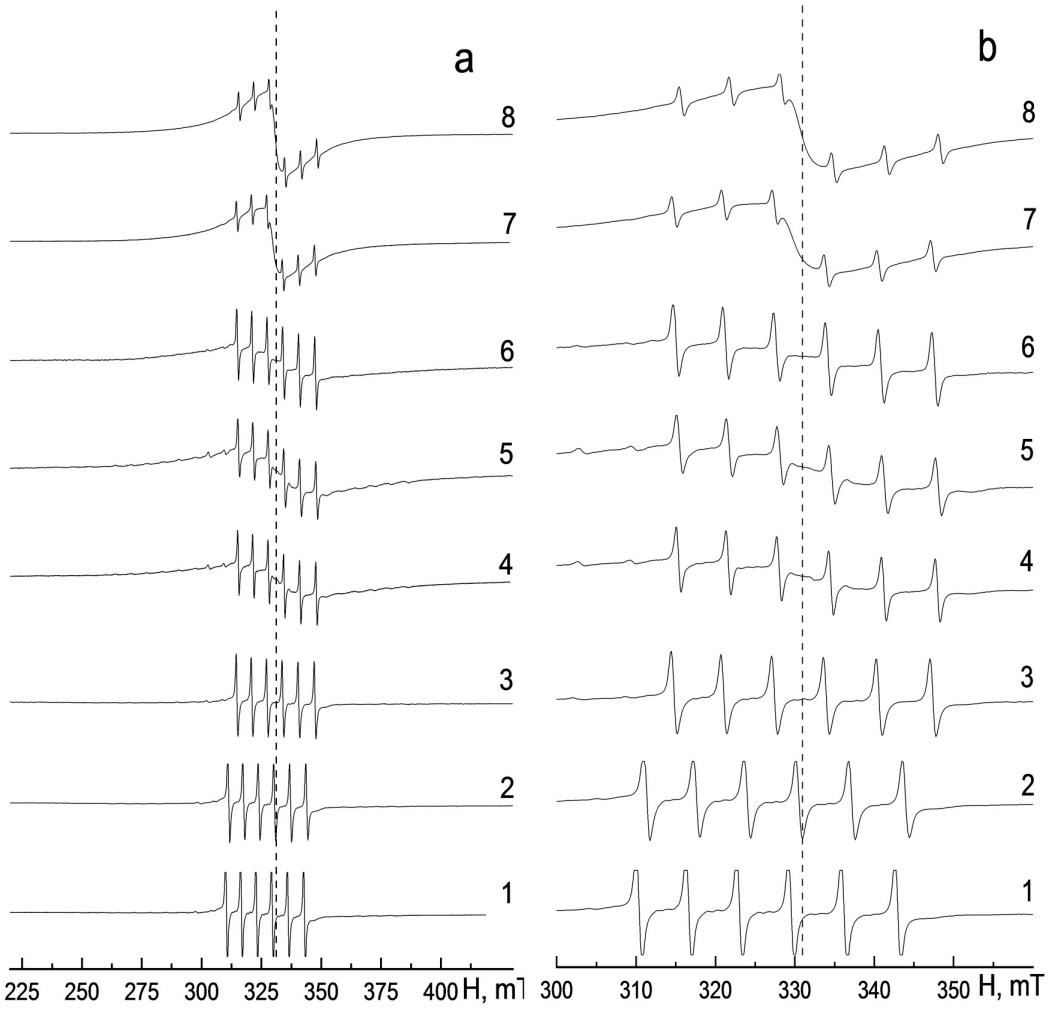

Fig. 2. EPR spectrum (a) and part of the spectrum (b) of ZnSe nanocrystals synthesized at a current of ~ 35A, during annealing in air: *1* — initial, *2* — annealing at 200°C, *3* — annealing at 300°C, *4* — annealing at 400°C, *5* — annealing at 500°C, *6* — annealing at 600°C, *7* — annealing at 700°C, *8* — annealing at 800°C.

On going from T = 600°C to T = 700°C, the intensity of the type (1) EPR spectrum of Mn^{2+} ions decreases by a factor of two, while the intensity of the EPR spectrum of type (2) increases. This can be explained by a decrease in the number of dislocations, since it is known that at small crystal sizes and T≥500°C, dislocations begin to move and emerge on the crystal surface [37].

The sum of the areas under the integral EPR spectrum increases at temperatures T≥400°C and reaches a maximum at a temperature T = 700–800°C. There are two possible reasons for this. Firstly, it is possible that during the annealing, part of the interstitial Mn which is in a different charge state with a large orbital momentum (for example, in interstices) is incorporated into the lattice and passes into the Mn^{2+} state. Secondly, during the combustion synthesis reaction, a larger amount of Mn can mainly be located in dislocations and, in this case, form antiferromagnetic pairs that do not give an EPR signal, while Mn spreads uniformly over the structure after annealing [38].

Figure 3b shows the dependence of the resonant value of the magnetic field due to Mn^{2+} ions and the hyperfine structure constant A of the EPR spectrum of Mn^{2+} ions on the annealing temperature. The hyperfine structure constant A = 6.56 mT with g-factor g = 2.007, associated with Mn^{2+} ions in a cubic environment, was determined for the original EPR spectrum. The maximum change in the g-factor occurs at T = 300°C: the hyperfine structure constant A = 6.35 mT and g = 2.005. The g-factor does not change during annealing at higher temperatures. For

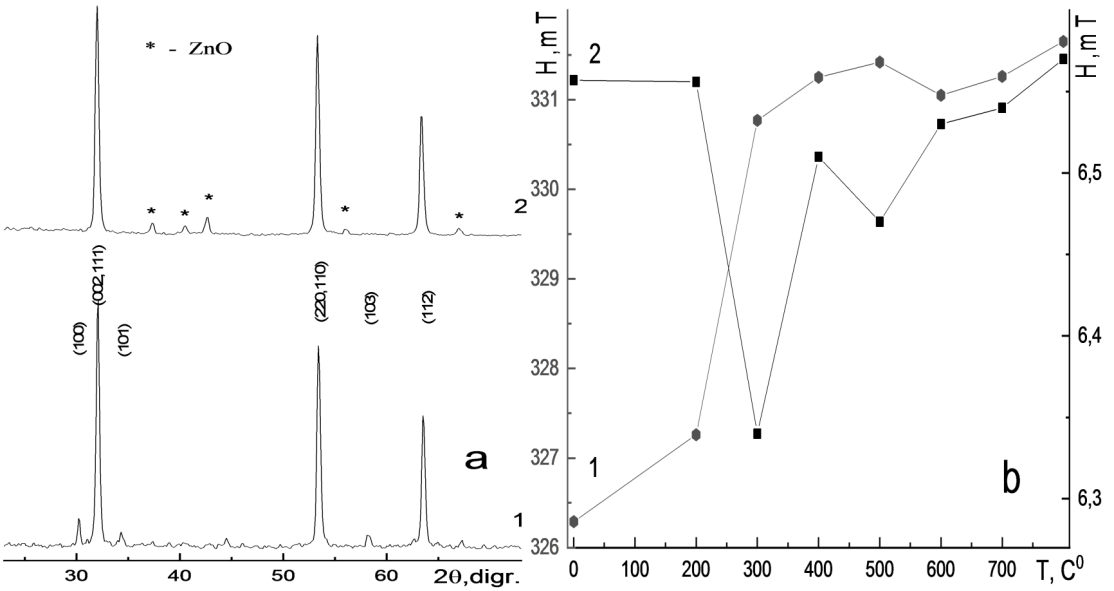

Fig. 3. XRD spectra (a) of ZnSe nanocrystals synthesized at a current of ~ 35 A, during annealing in air: *1* — initial; *2* — after annealing at T = 800°C; (b) dependences on the annealing temperature: the magnetic field resonant value of the six lines of the hyperfine structure absorption due to Mn^{2+} ions (1) and the hyperfine structure constant A (2) of the EPR spectrum of Mn^{2+} ions.

the EPR spectrum obtained after annealing at T = 800°C, the hyperfine structure constant A = 6.57 mT with g = 2.005 was determined. In [36], the values for the hyperfine structure of Mn^{2+} ions are shown as A = 6.09 mT and g = 2.007 for Mn^{2+} ions located in the matrix and up to A = 6.55 mT and g = 2.003 for Mn^{2+} ions located in bulk crystals. We obtained the values of the g-factor in this range, which indicates that the initial structure is closer in its composition to NCs, the structure after annealing is more uniform, and the composition is closer to that of bulk crystals.

The XRD data of ZnSe nanocrystals synthesized at a current of ~ 35 A are shown in Fig. 3a. It can be seen that the fraction of the cubic phase in ZnSe NCs is ~ (80÷5) % before annealing and ~ (95÷5) % after annealing. The structure of NCs has become more uniform after annealing. In the original sample, small amounts (~ 1–2 %) of additional phases (Se2O5 phase) were observed against the background. After thermal treatment, these phases disappeared, and the ZnO phase appeared (~ 3–4 %). Oxidation of ZnSe occurs during annealing above 426°C with the formation of the ZnO phase [39], which is seen in the XRD pattern; accordingly, to obtain purer ZnSe NCs with a homogeneous structure, it is more expedient to carry out annealing without the presence of oxygen, which we did in this work.

The sizes of NCs were determined by the Scherrer method. The average crystallite size increases from ~ 60 nm before annealing to ~ 80 nm after annealing, which may indicate that the higher the temperature, the larger the size of the nanocrystals. The degree of microstresses in the crystal lattice was estimated by broadening of the diffraction maxima: the microstresses decreased from $6.26 \cdot 10^{-4}$ before annealing to $3.77 \cdot 10^{-4}$ after annealing. The dislocation density calculated from the broadening of the lines of the diffraction pattern decreased from $4.41 \cdot 10^{10}$ to $3.52 \cdot 10^{10}$. The lattice parameter increased from 5.653 A before annealing to 5.657 A after annealing. This may be due to both an increase in the crystallite size and a decrease in the degrees of microstresses. The lattice parameter of bulk ZnSe crystals is 5.6687 A, and an increase in the lattice parameter during annealing was also noted by other researchers [40].

Fig. 4 shows the EPR spectra of ZnSe nanocrystals synthesized at a current of ~ 40 A during annealing in a nitrogen atmosphere. The spectrum also consists of the sum of spectra of types (1) and (2). A broad line of type (2) is immediately present in the initial EPR spectrum of ZnSe NCs. Perhaps, this may be due to the fact that the ZnSe NCs mainly have only a cubic structure, which we can see from the XRD data presented in Fig. 5a. The intensity of the

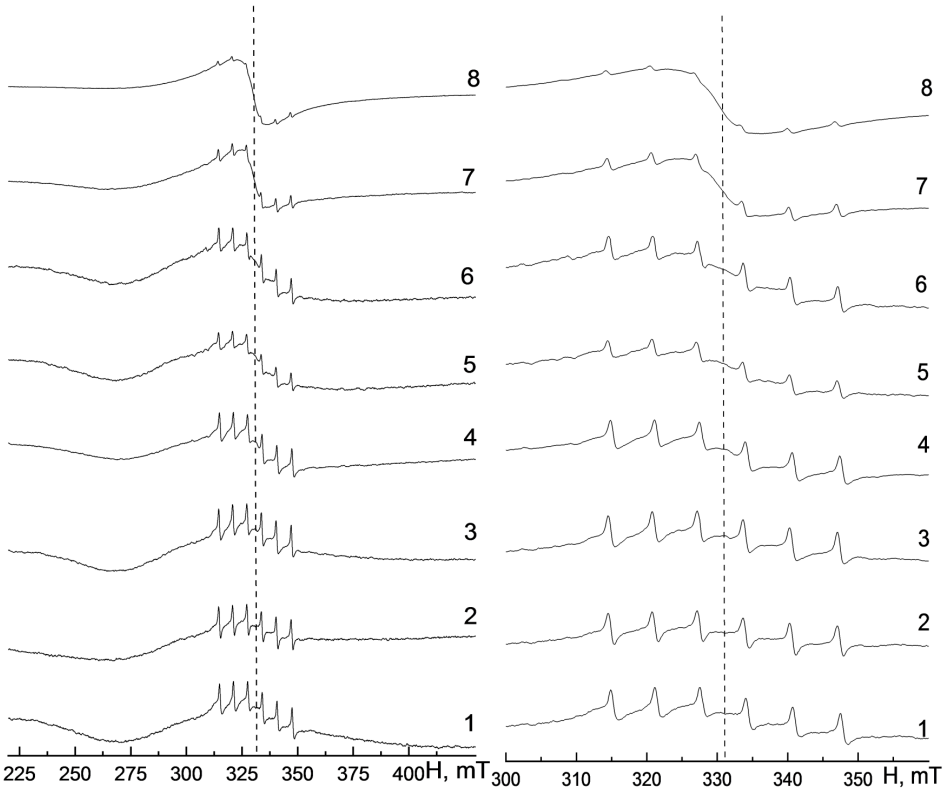

Fig. 4. EPR spectra (a) and part of the spectrum (b) of ZnSe nanocrystals synthesized at a current of ~ 40 A during annealing in nitrogen: *1* — initial, *2* — annealing at 200°C, *3* — annealing at 300°C, *4* — annealing at 400°C, *5* — annealing at 500°C, *6* — annealing at 600°C, *7* — annealing at 700°C, *8* — annealing at 800°C.

EPR spectra of types (1) and (2) in the range of $T = 0div400$°C changes insignificantly. This may be due both to a small number of dislocations and to the fact that the obtained ZnSe NCs have a more perfect cubic structure. The motion of dislocations can be observed at higher temperatures. In going from $T = 400$°C to $T = 500$°C, the intensity of the EPR spectra of Mn^{2+} ions of the type (1) decreases almost by a factor of two, and the signal of the type (2) increases, which may be due to the onset of the dislocation motion. Also, the intensity of the signal of the type (1) greatly decreases when going from $T = 600$°C to $T = 700$°C, while an increase in the signal of the type (2) is also observed. As we mentioned above, this can be easily explained by a decrease in the number of dislocations and their partial exit to the surface [37]. At $T = 800$°C, the intensity of the spectrum of Mn^{2+} ions during annealing in nitrogen is much lower than during annealing in oxygen. Most likely, this is due to the formation of a more perfect structure of ZnSe nanocrystals during annealing in nitrogen and the presence of a smaller number of defects than during annealing in air. Fig. 5b shows the dependence of the resonant value of the magnetic field due to Mn^{2+} ions and the hyperfine structure constant A of the EPR spectrum of Mn^{2+} ions on the annealing temperature. The g-factor is near $g = 2.005$ for all the temperatures. The hyperfine structure constants A of the EPR spectrum of Mn^{2+} ions are in the range of 6.4÷6.6 mT. The obtained values of the g-factor and constant A of the hyperfine structure of the EPR spectrum of Mn^{2+} ions are in the range presented in [36]. It indicates that the initial structure of the ZnSe nanocrystals synthesized at a current of ~ 40 A is more homogeneous in its composition and changes less at annealing than the structure of ZnSe NCs synthesized at a current of ~ 35 A.

The XRD patterns of ZnSe NCs synthesized at a current of ~ 40 A showed that the fraction of the cubic phase in ZnSe nanocrystals is ~ (90÷5) % before annealing and ~ (95÷5) % after annealing. The structure of NCs has become more uniform. The original sample did not contain any additional phases. The ZnO phase appeared

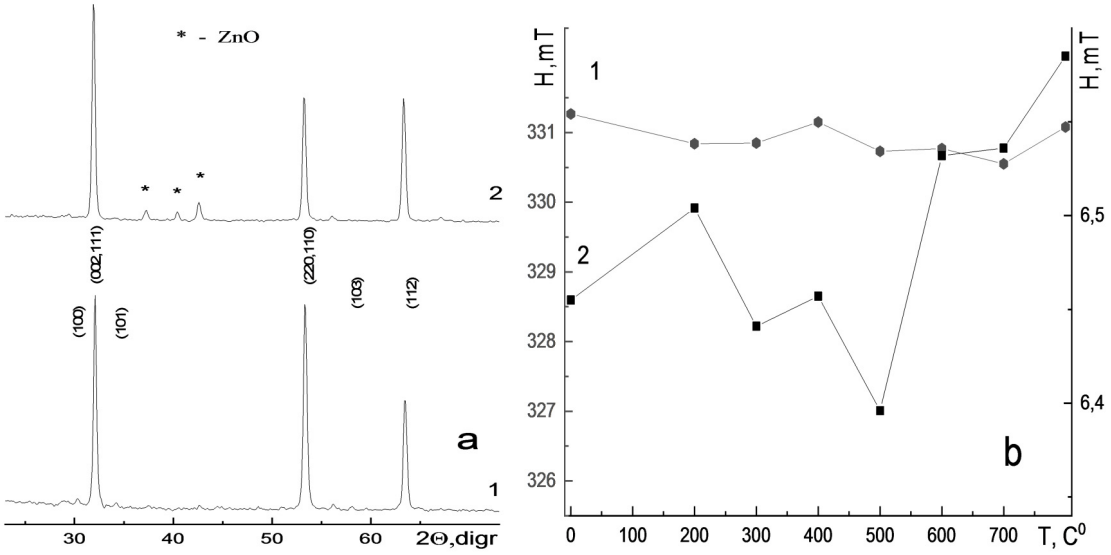

Fig. 5. (a) XRD spectra of ZnSe nanocrystals during annealing in nitrogen: *1* — initial, *2* — after annealing at T = 800°C; (b) dependence of the resonance value of the magnetic field of the broad absorption line due to Mn^{2+} ions (1) and the hyperfine structure constant A (2) of the EPR spectrum of Mn^{2+} ions on the annealing temperature.

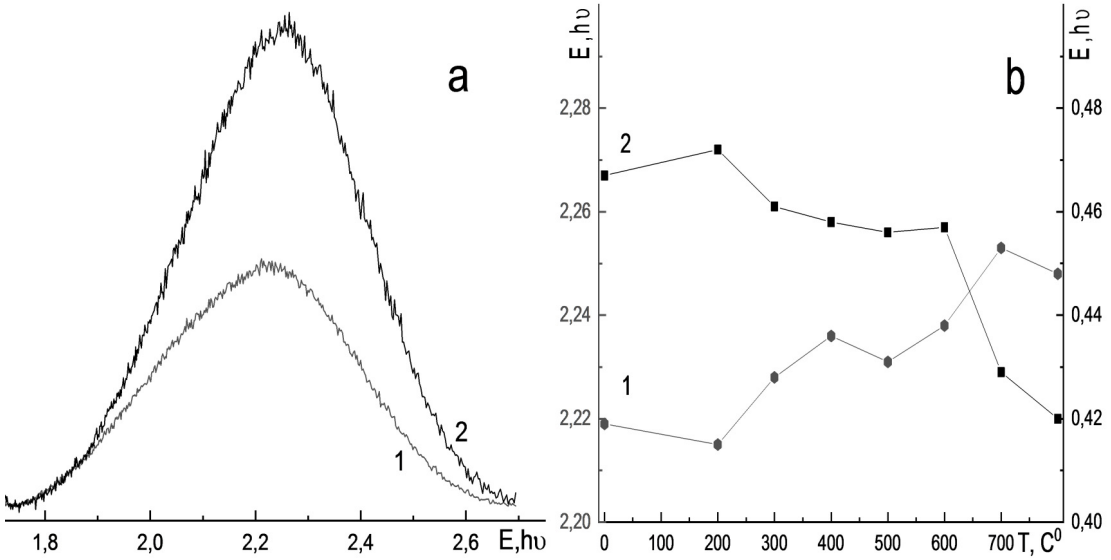

Fig. 6. (a) PL spectra of ZnSe nanocrystals: *1* — initial powder, *2* — powder after annealing at T = 800°C in air; (b) dependence of the location of the maximum (1) and half-width (2) of the integrated PL spectrum on the annealing temperature.

(~ 2–3 %) after the thermal treatment. Most likely, during annealing, interstitial oxygen in combination with zinc form the ZnO phase. However, the intensity of this phase during annealing in nitrogen vapor is lower than during annealing in air.

During annealing in a nitrogen atmosphere, the average crystallite size increased from 55 nm before annealing to 80 nm after annealing. Microstresses decreased from $6.57 \cdot 10^{-4}$ to $3.12 \cdot 10^{-4}$. The dislocation density decreased from $3.57 \cdot 10^{10}$ to $2.05 \cdot 10^{10}$. Also, the lattice parameter increased from 5.654 A to 5.659 A. This may be due to both an increase in the crystallite size and a decrease in the level of microstresses.

Summing up, we can conclude that in the temperature range from T = 0°C to T = 400°C, there is no change in the number of dislocations after annealing and slow cooling. This was also observed in [37]. In the temperature

range from $T = 500$°C to $T = 600$°C, the number of dislocations after annealing and slow cooling begins to decrease. However, this process has a small effect on the finite number of dislocations. This is most likely due to the fact that, upon slow cooling, dislocations can reappear, the number of which practically balances the number of dislocations that disappeared as a result of annealing. In the temperature range from $T = 700$°C to $T = 800$°C, the number of dislocations can decrease by orders of magnitude [37]. However, under slow cooling, new dislocations appear, although in a smaller amount. The behavior of dislocations during annealing and rapid cooling requires a detailed study, since the appearance of more perfect structures, although nonequilibrium, is possible.

We have already considered the PL spectra of ZnSe NCs [33, 41], however their behavior during annealing reveals previously unknown information. Figure 7 shows the PL spectra of ZnSe NCs synthesized at a current strength of ~ 35 A and after annealing in air at $T = 800$°C; also the dependence of the location of the maximum (1) and a half-width (2) of the integral PL spectrum on the annealing temperature are shown. As can be seen, during annealing, the maximum smoothly shifts towards higher energies; the greatest change is observed in the range $T = 600 div 700$°C, which may confirm our assumption about the emergence of dislocations on the surface in this temperature range. The spectrum becomes noticeably narrower after annealing, which indicates a greater homogeneity of the structure. Note that after annealing, the integral intensity of the PL spectrum noticeably increases. In this work, we did not decompose the integral PL spectrum into elementary bands, as we did in [42, 43], using smoothing methods based on the Tikhonov method and the derivative spectroscopy method, since the behavior of elementary bands can shift the emphasis and give redundant information.

Summing up, it is possible to determine the scope of the ZnSe NCs synthesized by the combustion synthesis method, and especially those obtained as a result of annealing. It is possible to obtain NCs with sizes of about 4 nm both from the ZnSe NCs synthesized by us, (the production technology is described in [30]), and hot-pressed ceramics of the Cleartran or Multispectral classes [44]. This allows them to be used both in any optoelectronic devices and in some areas of the military industry, for example, thermal imagers or durable protective coatings [45]. Nowadays, most of the obtained Cleartran or Multispectral class ZnSe ceramics are produced by chemical vapor deposition (CVD) [46] and spark plasma sintering (SPS) [47]; however, these processes are long-standing and complex. In addition, the production of ceramics by CVD and SPS methods is very expensive, and the resulting crystals are quite brittle. Therefore, it is expedient to produce ZnSe NCs by the combustion method, and then to use them for obtaining military ceramics by hot pressing.

4. Conclusions

In order to improve the spectroscopic properties of ZnSe NCs, a series of thermal annealings of ZnSe NCs synthesized by the combustion method was carried out. The developed approach allows obtaining the ZnSe NC material with desired properties by controlling its crystalline structure. This opens prospects for further application of this material in hot-pressed ceramics of the Cleartran and Multispectral classes. During annealing, the NC size increases by ~ 20 %, the fraction of the cubic phase grows, and the lattice parameter also increases compared to the initial state. During annealing, the NC structure becomes more perfect, the number of dislocations and microstresses decrease. A rational choice of heat treatment regimes makes it possible to obtain materials with a given structure [48–50] and the required set of properties [51–53]. During annealing, the ZnO phase appears both in air and in a nitrogen environment, while the amount of ZnO formed in a nitrogen environment is much less. From the initial EPR spectrum of ZnSe NCs, the hyperfine structure constant $A = 6.26$ mT and the g-factor $g = 2.007$ associated with Mn^{2+} ions in a cubic environment were determined. The maximum change of the g-factor occurs at $T = 300$°C; the hyperfine structure constant becomes $A = 6.35$ mT and $g = 2.005$. The g-factor does not change during annealing at higher temperatures.

References

1. V.S.Vahrusheva, D.B.Hlushkova, V.M.Volchuk et al., *Problems of Atomic Science and Technology*, **140**, 4 (2022).
2. P.H.Binh, N.T.Hung, *IEEE Photonics Technology Letters*, **28**, 18 (2016).
3. Qi Zhang, Huiqiao Li, Ying Ma et al., *Progress in Materials Science*, 83 (2016).

4. S.Jagtap, P.Chopade, S.Tadepalli et al., *Opto-Electronics Review*, **27**, 1 (2019).
5. S.Galkin, I.Rybalka, L.Sidelnikova et al., *Journal of Luminescence*, 239 (2021).
6. X.Ropagnol, R.Morandotti, T.Ozaki et al., *IEEE Photonics Journal*, **3**, 2 (2011).
7. I.Dmitruk, N.Berezovska, V.Degoda et al., *Journal of Nanomaterials*, 2021 (2021).
8. U.Choudhari, S.Jagtap, *Journal of Electronic Materials*, 49 (2020).
9. A.O.Sofiienko, V.Y.Degoda, *Radiation Measurements*, **47**, 1 (2012).
10. V.K.Nguyen, D.K.Pham, N.Q.Tran et al., *Green Processing and Synthesis*, **11**, 1 (2022).
11. M.H.Abib, X.Yao, G.Li et al., *Nano*, **11**, 08 (2016).
12. B.Feng, J.Cao, D.Han et al., *Materials Science in Semiconductor Processing*, 27 (2014).
13. A.Chauhan, A.Sudhaik, P.Raizada et al., *Process Safety and Environmental Protection*, 170 (2023).
14. C.Sun, Y.Gu, W.Wen et al., *Optical Materials*, 81 (2018).
15. M.Chinnasamy, R.Rathanasamy, S.Sivaraj et al., *Journal of Electronic Materials*, **51**, 6 (2022).
16. D.Li, N.Wei, J.Yang et al., *Optical Materials*, 132 (2022).
17. J.K.Zhang, J.M.Shi, D.P.Zhao et al., *Optical Engineering*, **56**, 7 (2017).
18. X.Peng, F.Ai, L.Yan et al., *Cell Reports Physical Science*, **2**, 5 (2021).
19. S.Dehghani, N.K.Nasab, M.Darroudi, *Nanomedicine Journal*, **9**, 1 (2022).
20. A.Pawlis, G.Mussler, C.Krause et al., *ACS Applied Electronic Materials*, **1**, 1 (2018).
21. M.Godlewski, E.Guziewicz, K.Kopalko et al., *Journal of Luminescence*, 102 (2003).
22. S.R.Vangala, D.Brinegar, V.L.Tassev et al., *Journal of Crystal Growth*, 522 (2019).
23. E.A.Mironov, O.V.Palashov, S.S.Balabanov, *Optics Letters*, **46**, 9 (2021).
24. H.Sirringhaus, N.Tessler, R.H.Friend, *Science*, **280**, 5370 (1998).
25. T.Rakshit, S.Mandal, P.Mishra et al., *Journal of Nanoscience and Nanotechnology*, 12 (2012).
26. A.J.Varkey, A.F.Fort, *Solar Energy Materials and Solar Cells*, **29**, 3 (1993).
27. H.-C.Chiu, C.-S.Yeh, *The Journal of Physical Chemistry C*, **111**, 20 (2007).
28. E.A.Levashov, A.S.Mukasyan, A.S.Rogachev et al., *International Materials Reviews*, **62**, 4 (2017).
29. A.S.Rogachev; A.S.Mukasyan, Combustion for Material Synthesis, CRC Press (2014).
30. Y.Y.Bacherikov, A.V.Gilchuk, A.G.Zhuk et al., *Journal of Luminescence*, 194 (2018).
31. G.Liu, X.Yuan, J.Li et al., *Materials & Design*, 97 (2016).
32. Z.Tian, Z.Chen, X.Yuan et al., *Ceramics International*, **45**, 14 (2019).
33. Y.Plakhtii, O.Khmelenko, *Physica Scripta*, **98**, 3 (2023).
34. A.V.Kovalenko, Y.G.Plakhtii, O.V.Khmelenko, *Functional Materials*, **25**, 4 (2018).
35. I.Borovinskaya, A.Gromov, E.A.Levachov et al., ??? Elsevier (2017).
36. D.S.Mazing, A.V.Nikiforova, A.S.Osinin et al., *Applied Magnetic Resonance*, 48 (2017).
37. X.G.Zhang, I.A.Rodriguez, P.Li et al., *Journal of Electronic Materials*, 30 (2001).
38. N.E.Korsunska, Y.Y.Bacherikov, T.R.Stara et al., *Semiconductors*, 47 (2013).
39. M.Verma, A.Kaswan, D.Patidar et al., *Journal of Materials Science: Materials in Electronics*, 27 (2016).
40. V.I.Voronin, I.F.Berger, N.V.Proskurnina et al., *The Physics of Metals and Metallography*, 117 (2016).
41. A.V.Kovalenko, Y.G.Plakhtii, O.V.Khmelenko, *Journal of Nano- and Electronic Physics*, **11**, 4 (2019).
42. A.V.Kovalenko, S.M.Vovk, Y.G.Plakhtii, *Functional Materials*, **27**, 2 (2020).
43. A.V.Kovalenko, S.M.Vovk, Y.G.Plakhtii, *Ukrainian Journal of Physical Optics*, **19**, 3 (2018).
44. G.R.Durand, N.Hakmeh, V.Dorcet et al., *Journal of the European Ceramic Society*, **39**, 10 (2019).
45. D.C.Harris, Window and Dome Technologies and Materials, 6545 (2007).
46. D.C.Harris, M.Baronowski, L.Henneman et al., *Optical Engineering*, **47**, 11 (2008).
47. C.Chlique, G.Delaizir, O.Merdrignac-Conanec, *Opt. Mater.*, 33 (2011).
48. N.E.Kalinina, D.B.Glushkova, A.I.Voronkov et al., *Functional Materials*, **26**, 3 (2019).
49. D.B.Hlushkova, V.A.Bagrov, S.V.Demchenko et al., *Problems of Atomic Science and Technology*, **140**, 4 (2022).
50. D.B.Hlushkova, V.A.Bagrov, V.M.Volchuk et al., *Functional Materials*, **30**, 1 (2023).
51. D.Klets, I.V.Gritsuk, A.Makovetskyi et al., *SAE Technical Papers*, 2018-01-0015 (2018). https://saemobilus.sae.org/content/2018-01-0015/
52. M.Podrigalo, A.Turenko, V.Bogomolov et al., *SAE Technical Papers*, 2018-01-1880 (2018). https://saemobilus.sae.org/content/2018-01-1880/
53. M.Mikhalevich, A.Yarita, A.Turenko et al., *SAE Technical Papers*, 2018-01-1295 (2018). https://saemobilus.sae.org/content/2018-01-1295/